JOURNAL OF MAGNETIC RESONANCE **125,** 325–331 (1997)
ARTICLE NO. MN971124

Radial Spectroscopic Imaging

M. MEININGER,* P. M. JAKOB,* M. VON KIENLIN,* D. KOPPLER,† G. BRINGMANN,† AND A. HAASE*

*Lehrstuhl für Experimentelle Physik V, and †Lehrstuhl für Organische Chemie I, Universität Würzburg, Am Hubland, 97074 Würzburg, Germany

Received December 16, 1996

A family of fast chemical-shift imaging techniques, which takes advantage of the cylindrical symmetry found, for instance, in some plants, is introduced. Variants with one and two spectral dimensions allow rapid measurement of the radially dependant spatial distribution of metabolites in such objects. Compared to conventional chemical-shift imaging and correlation-peak imaging, the minimal experimental duration can be reduced substantially. The impact on the SNR is discussed. Radial spectroscopic ^{1}H NMR images of metabolites in *Ancistrocladus heyneanus,* a tropical liana plant, are shown, using both radial chemical-shift imaging and radial correlation-peak imaging. The spatial distribution of various metabolites in this plant have been measured. The reduction of experimental duration compared to the conventional techniques was by a factor of 63 and 31, respectively.

INTRODUCTION

Chemical-shift imaging (CSI) is a method used to investigate the regional metabolism of biological objects (*1, 2*). One complete NMR spectrum is obtained for each volume element. This technique allows noninvasive acquisition of information on the distribution of metabolites in biological systems *in vivo.* In medical applications, CSI has been mainly used for investigations of metabolism in the brain (*3–5*), and the heart (*6–8*). In recent years, some studies have shown that CSI can also be applied to study plant histochemistry. It has been used to reveal qualitative information on water and lipid distribution in fennel seeds (*9*). Quantitative measurements have been done on the sucrose distribution in *Ricinus communis* seedlings (*10*). All these measurements can be done noninvasively under well-controlled environmental conditions, allowing repetitive studies on the same plant individual.

Especially when a large number of metabolites are present, a one-dimensional NMR spectrum is often inadequate to identify metabolites due to excessive line overlap. Two-dimensional NMR spectroscopy is a standard tool for the identification and characterization of chemical structures. It allows identification of metabolites by their correlation peaks in a two-dimensional spectrum. In order to combine these possibilities with spatial resolution, the standard CSI approach with one spectroscopic acquisition dimension has been extended to the correlation-peak-imaging (CPI) experiment with two spectroscopic and two spatial dimensions (*11, 12*). With this technique, it was possible to localize a large number of metabolites in *R. communis* seedlings (*11, 12*) and rat brains (*13*) *in vivo.* The disadvantage of the CPI technique lies in its long experiment time due to the large number of acquisition dimensions.

In magnetic-resonance imaging, two methods have been suggested to reduce the acquisition time of an image if the object has a cylindrical symmetry. In this case, only the radially dependent spatial information needs to be measured. One method is to make use of a radial-magnetic field gradient, i.e., a gradient which produces a radially dependant magnetic field gradient (*14, 15*). The other performs acquisition of one-dimensional projections followed by an inverse Abel transform (IAT) to obtain radial profiles (*16*). The advantage of the latter technique is that there is no need for extra hardware and that the needed postprocessing routines are easy to implement.

In this paper, we demonstrate that radial imaging can be combined with one- or two-dimensional spectroscopic experiments, leading to a reduction of acquisition dimensions and experiment duration in comparison to CSI and CPI. In the following, we will call this approach radial chemical-shift imaging and radial-correlation-peak imaging (*17*). It should be noted that ''radial'' imaging refers to the ''real'' imaging dimensions and not a circular *k*-space sampling. We will use the term ''spectroscopic imaging'' as a generic term for CSI and CPI. Radial spectroscopic imaging is especially suitable for studies on plant systems with cylindrical stem symmetry. As an example, we present radial spectroscopic images of metabolites in *Ancistrocladus heyneanus,* an Indian liana plant, which we investigate because of its pharmacologically interesting alkaloids (*18*).

A similar approach, using one-dimensional projections and IAT for radial spectroscopic imaging, has been proposed by Schiffenbauer *et al.* (*19*). For practical application of this method on tumor cell spheroids, they performed a fitting of a model function to the measured profiles instead of application of the IAT.

1090-7807/97 $25.00

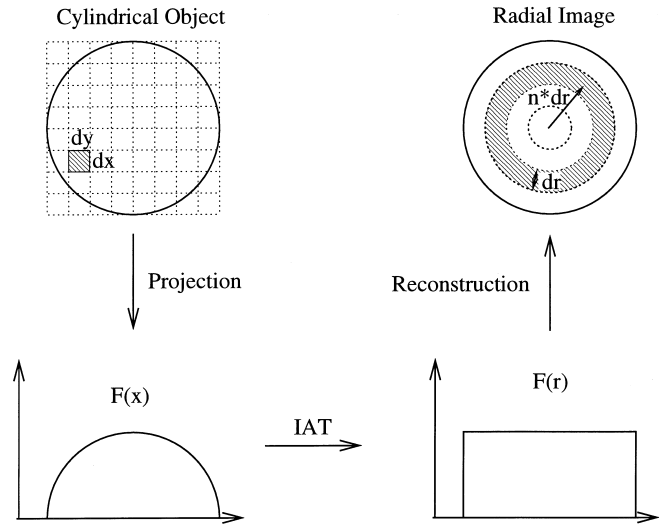

FIG. 1. The principle of radial-spectrocopic imaging: The one-dimensional projection $F(x)$ of a cylindrical object is measured for each spectroscopic point. The inverse Abel transform reconstructs the radial profile $F(r)$. From this, a radial-spectroscopic image can be reconstructed for better comparability. The pixel size in the radial-spectroscopic image is $2\pi n_r \Delta r \Delta r$ compared to $\Delta x \Delta y$ in the conventional image.

THEORY

If the system under investigation has cylindrical symmetry, it is possible to exploit this symmetry in order to reduce the number of spatial acquisition dimensions by one. If we describe the image plane in cylindrical coordinates $F = F(r, \theta)$ and the object has a cylindrical symmetry, i.e., $\partial F/\partial\theta = 0$, then the radial profile $F(r)$ contains complete spatial information. To obtain these profiles, we use the technique illustrated in Fig. 1, based on the same principal as fast radial imaging (*16*).

For an object with cylindrical symmetry, there exists a unique relation between its one-dimensional projection $F(x)$ and the radial profile $F(r)$. This relation is the inverse Abel transform (*20*):

$$F(r) = \int_r^\infty \frac{F'(x)dx}{\sqrt{x^2 - r^2}}. \qquad [1]$$

By combining standard spectroscopic experiments with phase encoding in one direction, we obtain the one-dimensional projections. After inverse Abel transformation, we get the radial profiles for each spectroscopic point, which can then be taken to reconstruct radial spectroscopic images. This results in pixels having the shape of concentric rings with uniform radial resolution. The reconstructed radial spectroscopic images contain no additional information compared to the radial profiles but allow a direct comparison to conventional images.

The reason for the possible time savings with radial spectroscopic imaging is the following: in spectroscopic imaging, the measuring time for a given signal-to-noise ratio (SNR) depends on the pixel volume. For radial spectroscopic imaging, the radially dependent pixel size is (see Fig. 1)

$$A_{\text{radial}}(r) = 2\pi r \Delta r = 2\pi n_r (\Delta r)^2, \qquad [2]$$

with n_r being the nth pixel from the center. This can be compared to the pixel size in the conventional image

$$A_{\text{conv}} = \Delta x \Delta y. \qquad [3]$$

Assuming that

$$\Delta x = \Delta y = \Delta r \qquad [4]$$

the radially dependant pixel size in the radial image is

$$A_{\text{radial}}(r) = 2\pi n_r A_{\text{conv}}. \qquad [5]$$

The nth pixel in the radial image is $2\pi n_r$ times larger than the pixels in a conventional image with same spatial resolution. The larger pixel size is the reason for the possible time saving for radial spectroscopic imaging compared to conventional SI. The radially dependent pixel size causes a radially dependent SNR. The standard deviation of the noise after IAT is not proportional to n_r^{-1}, as might be expected, but to $n_r^{-0.5}$ (*16*). This is because according to [1], the signals $F(x)$ do not contribute equally to the radial profile $F(r)$.

Biological objects never have perfect cylindrical symmetry. Thus, it is necessary to use a method which is robust when deviations from the cylindrical symmetry are present. Major *et al.* showed that the method described is relatively robust when small deviations from cylindrical symmetry are present in the object. They only lead to spatially limited perturbations in the images (*16*). This fact allows this method to be employed for *in vivo* applications.

MATERIALS AND METHODS

SNR Simulation

In order to examine the SNR behavior of this method, we performed a Monte Carlo simulation. One thousand 64 × 64 pixel images with signal intensity 1 were created. Noise with a standard deviation of 0.01 was added to each image. This simulates images with a SNR of 100. These images were then Fourier transformed. This data represents the *k*-space data for a two-dimensional imaging experiment. The

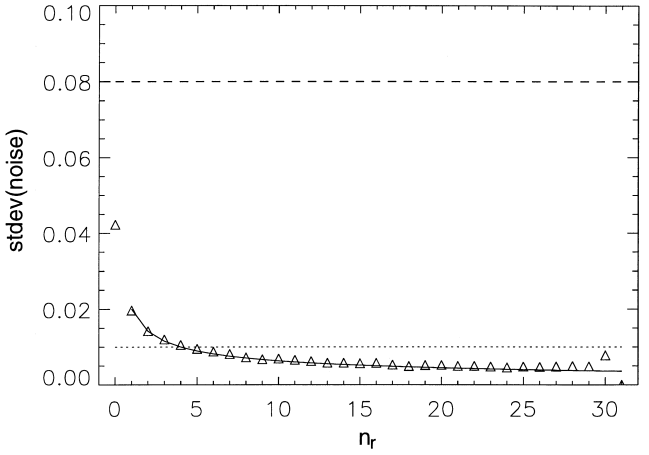

FIG. 2. Monte Carlo simulation of the radially dependant noise level in radial imaging. The standard deviation of the noise is shown, depending on the number of the pixel n_r, counted from the center of the image. The triangles show the simulated data for the radial image, the solid line the theoretical $n_r^{-0.5}$ curve. The horizontal lines represent the noise in the corresponding conventional image with 64 × 64 pixels and same acquisition time (dashed), and 64 times the acquisition time (dotted) of the radial image.

$k_x = 0$ lines represent the data acquired in a radial imaging experiment. They were selected and transformed back to obtain the one-dimensional profiles in real space. After application of IAT, the radial profiles were obtained and again normalized to a signal intensity of 1. Finally, the radially dependent standard deviation of the signal was calculated. This equals the noise level or inverse of the SNR which can then be compared to the initial value.

NMR Measurements

We have tested our method on a phantom with cylindrical symmetry, consisting of two concentric glass tubes. The inner tube is filled with water, the outer tube with a 500 mM sucrose solution (see Fig. 2). For an *in vivo* test of the method, we used *A. heyneanus*, a delicate, but rewarding tropical plant species, which has been cultivated for the first time in Würzburg (*18*). The condition of cylindrical symmetry is well satisfied in the shoot of this plant (see Fig. 4). At the age of about 1 year, the plant undergoes a phase of rapid shoot elongation. At this stage, the shoot reaches a state which is ideal for *in vivo* NMR investigations. It has a large diameter and long internodes (i.e., the distance between the leaf rudiments). Due to the fast growth, the material is not as woody as tissues from slowly growing plant material. This leads to relatively long T_2^* values resulting in a small linewidth of 20 Hz in the *in vivo* spectra.

The NMR experiments were performed on a 7 T Bruker Biospec 70/20 spectrometer. Gradient coils were capable of achieving gradients up to 200 G/cm with rise and fall times less than 200 μs. A Bruker microimaging probe head was used. We used a spin-echo pulse sequence with additional CHESS water suppression (*21*) for CSI and radial chemical-shift imaging. Slice selective 500 μs Gauss-shaped pulses were used. The data set had 512 spectroscopic points. The number of phase-encoding steps in any spatial direction was 31 for the phantom experiment and 63 for the *in vivo* experiment, allowing symmetric *k*-space sampling (*22*). The echo time (T_E) was 7 ms and the repetition time (T_R) was 1.3 s.

Radial-correlation-peak imaging used a COSY pulse sequence with pulsed field gradients (*23*). The first 90° pulse was a slice-selective 500 μs Gauss-shaped pulse, while the second pulse was an 18 μs hard pulse. Radial-correlation-peak Imaging data set had 256 × 64 spectroscopic points with a minimum t_1 of 4.8 ms and 31 phase-encoding steps.

All data were zero-filled to 32 or 64 spatial points, respectively, and Hanning filtered in spatial direction. A matched exponential filter was applied to one-dimensional spectra. The absorptive part of phase-corrected spectra is displayed. Two-dimensional spectroscopic data were filtered with a sine-bell filter in f_1 and a moving Hanning filter in f_2. Two-dimensional spectra are displayed in magnitude mode.

After Fourier transformation, radial-spectroscopic-imaging data were zero-filled to 128 spatial points. Afterward, the object was shifted to the center of the acquisition window. It should be noted that because of this processing step, the object needs not exactly be centered in the FOV during the measurement. The left and right parts of the profiles were added, and finally the inverse Abel transform was applied. If averaging of several experiments is necessary, it is possible to rotate the projection direction in steps of, e.g., 45°. By adding the different projections, it is possible to average out deviations from the cylindrical symmetry, like slight gradients on the signal intensity in one direction of the image plane. This procedure was used for the radial-correlation-peak Imaging measurement on *A. heyneanus.*

Sweepwidth was 1.5 kHz for the phantom measurements and 3.0 kHz for the measurements on the plant material. For the phantom experiments and the radial-correlation-peak-imaging experiment on *A. heyneanus*, the FOV was 7 mm, leading to a spatial resolution of 340 μm (31 spatial points, Hanning filter). For the radial-chemical-shift-imaging measurement on the liana stem, the FOV was 9 mm, leading to a spatial resolution of 210 μm (63 spatial points, Hanning filter). All measurements were made at room temperature.

RESULTS

Figure 2 shows the result of the Monte Carlo simulation. The radially dependent noise levels in the radial image are in the range of 0.005 and 0.042 compared to 0.01 in the conventional image. They are in good agreement to the theoretical $n_r^{-0.5}$ function. Except for the first few points, the

values are smaller than the value of 0.01 for the conventional image, although the experiment time is 64 times shorter in a radial-imaging experiment. Assuming the same experiment time, the noise level of the conventional experiment would have been $0.01 \times \sqrt{64} = 0.08$. Thus, the gain in SNR per-time is in the range of 2 (center of the image) to 16 (edge of the image) for this example.

Figure 3a shows a ^{1}H NMR spin-echo image of the phantom. The two compartments can be seen which have a slight shift from a perfect concentric position. Figure 3b shows a COSY spectrum of the phantom. A cross peak can be seen, correlating the resonances at 5.3 and 3.6 ppm. Taking the intensity of this peak as the spectroscopic information and processing the radial-correlation-peak-imaging data as described, one obtains the image in Fig. 3c. The radial information on the sucrose distribution in the phantom is fully reproduced. Because of the small sensitivity of the 2D spectroscopic experiment, the SNR was relatively poor. The noise which appears in this image has the form of concentric rings, according to the pixel shape.

The ^{1}H NMR spin-echo image (see Fig. 4a) shows the different concentric regions of the stem of *A. heyneanus*. The condition of cylindrical symmetry is well satisfied so that this object is suitable for radial-spectroscopic imaging. Figure 5 shows one-dimensional NMR spectra of the plant stem. Besides the residual water signal at 4.8 ppm, a number of resonances can be detected which can be tentatively assigned to aromatic compounds (6–8 ppm), sugars (3–4 ppm), and aliphatic compounds (0–3 ppm). Due to the relatively broad linewidth of 20 Hz, the lines from different metabolites overlap. Thus, an exact assignment of resonances to specific compounds is difficult. For instance, Fig. 4b shows the distribution of the sugar peak taken from a conventional CSI experiment. The experiment time was $11\frac{1}{2}$ h due to the high spatial resolution of 63×63 pixels and 8 averages. It shows high intensity in the phloem region, lower intensity in the pith region, and very low intensity in the xylem region. The corresponding radial-chemical-shift image (Fig. 4c) of the sugar peak reveals the same information: high intensity in the phloem region, lower in the pith region, and small in the xylem region. In this case, the measuring time is reduced from $11\frac{1}{2}$ h to 11 min with equivalent radial resolution and no penalty in SNR. Figure 5 compares spectra from the same sample for the radial and the conventional techniques. They are taken from the phloem and the outer pith regions of the plant, both at the same radii from the center. The spectra are in good agreement. The relative amplitudes of different resonances are correctly reproduced in the spectra obtained using the radial technique. Again the SNR is similar with both techniques.

Figure 6a shows a two-dimensional COSY spectrum of a shoot of *A. heyneanus.* A number of cross peaks can be seen.

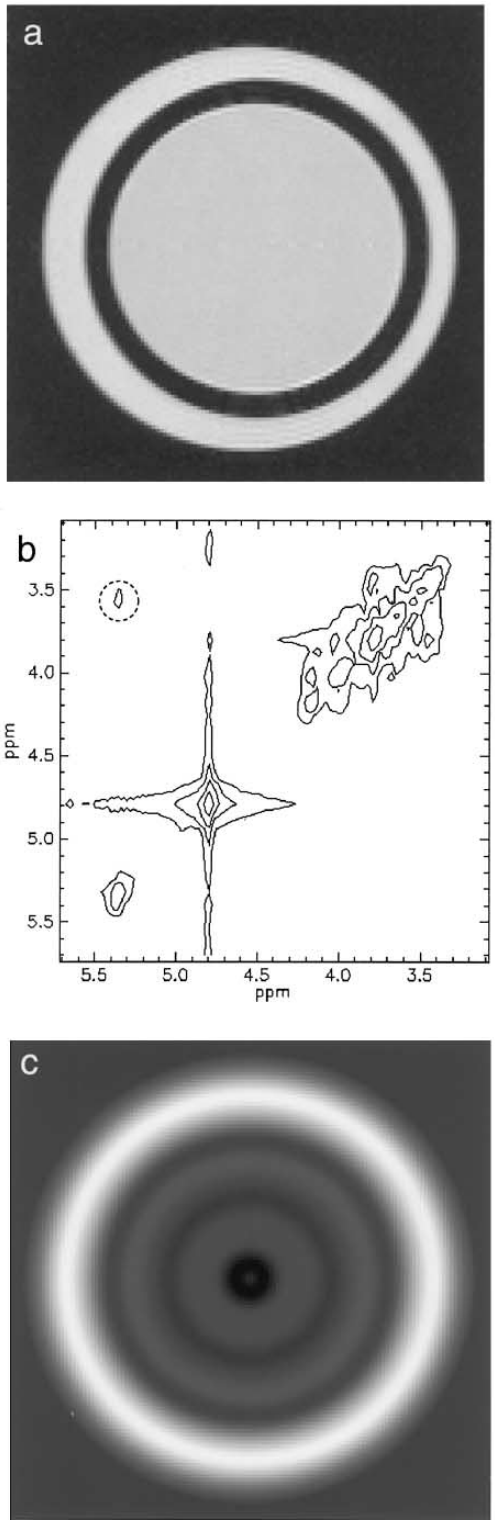

FIG. 3. (a) ^{1}H NMR spin-echo image of the phantom (128×128 image matrix, FOV = 7 mm, 2 mm slice thickness, T_E = 11 ms, T_R = 1 s). The inner tube is filled with water, the outer tube with a 500 mM sucrose solution. (b) COSY spectrum with typical sucrose cross peak, and (c) radial-correlation-peak image of sucrose in the phantom.

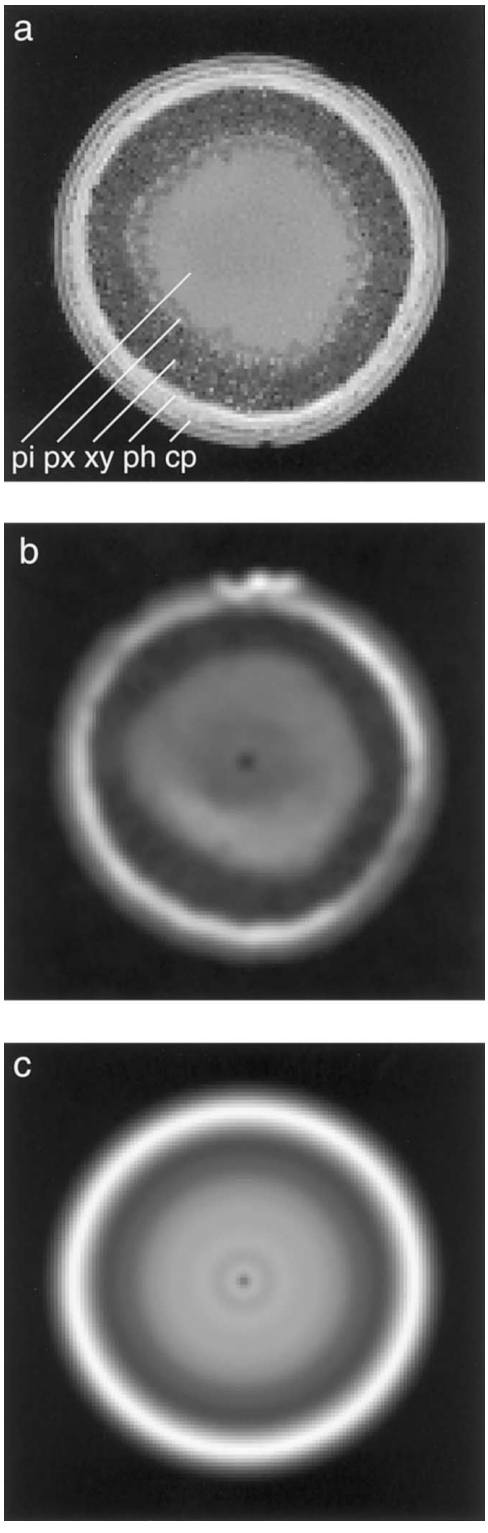

FIG. 4. *Ancistrocladus heyneanus:* (a) ^{1}H NMR spin-echo image of shoot (128 × 128 image matrix, FOV = 9 mm, 2 mm slice thickness, T_E = 7 ms, T_R = 1 s). The plant tissues are pi = pith, px = protoxylem, xy = xylem, ph = phloem, cp = cortex parenchyma. (b) CSI of sugar peak, and (c) radial-chemical-shift image of sugar peak.

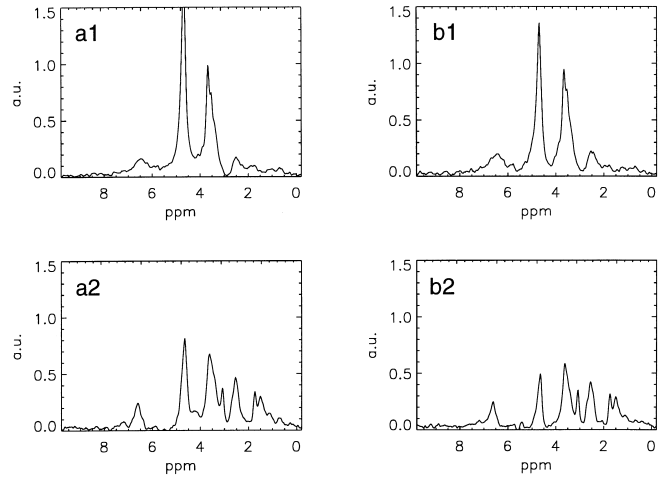

FIG. 5. Comparison of ^{1}H spectra from (a) radial-chemical-shift imaging and (b) conventional CSI, taken out of (1) the phloem region, and (2) the outer pith region.

We are especially interested in the metabolite corresponding to the cross peak which correlates with the resonances at 7.3 in the aromatic region and 3.2 ppm in the aliphatic region. This metabolite has not been identified until now. The spatial distribution of the metabolite was obtained from a radial-correlation-peak-imaging data set (Fig. 6b). The metabolite appears only in the pith region of the plant. The experiment time was 10 h, compared to 13 days for a comparable experiment using CPI.

DISCUSSION

The results of the Monte Carlo simulation showed that the SNR in a radial imaging experiment is roughly the same as in a comparable conventional imaging experiment with the same number of averages. The shorter experiment time is compensated by the larger pixel size in the radial imaging experiment. The same is valid for radial-spectroscopic-imaging experiments for every single spectroscopic point. It should also be noted that under the condition of cylindrical symmetry there is no loss in spatial information.

The results of the phantom study prove the ability of radial-spectroscopic imaging to measure the distribution of chemical constituents using 2D spectroscopic experiments. The appearance of noise in the form of concentric rings should be noted. The radial-correlation-peak image of the sucrose had a rather poor SNR but the image still shows the correct spatial distribution.

The good correspondence of the conventional and the radial-chemical-shift image of sugars in *A. heyneanus* proves that this method works even in real objects, where the cylindrical symmetry is only fulfilled approximately. Besides radial-spectroscopic images of spectral components, spectra

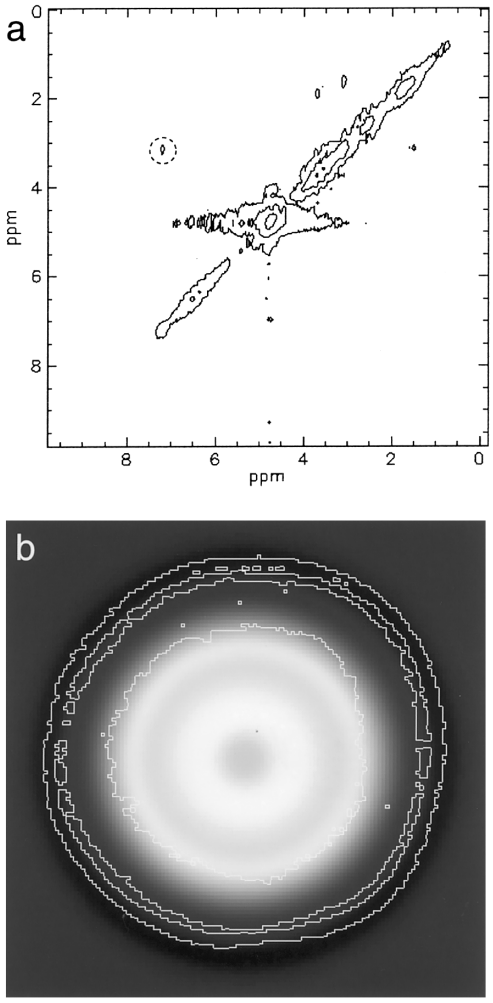

FIG. 6. (a) COSY spectrum of shoot of *Ancistrocladus heyneanus* with investigated cross peak, and (b) radial-correlation-peak image of corresponding metabolite with overlayed contour plot of conventional NMR image similar to Fig. 4a.

from certain radii are correctly reproduced. This allows comparison of spectra from different parts of the object.

Radial-correlation-peak imaging allows acquisition of spatially resolved 2D spectroscopic information in cases where a conventional technique, like CPI, could not be applied due to the long experiment time required for sufficient SNR. The application to the sensitive tropical liana *A. heyneanus* shows the great value of this method. The 1D spectra make an unequivocal identification of metabolites difficult due to excessive line overlap. Radial-correlation-peak imaging alleviated this problem. It allowed detection of a hitherto unidentified metabolite in the plant and measurement of its radial distribution. We are now attempting to identify it by means of high-resolution NMR on plant tissue extracts.

CONCLUSION

The present results prove the capacity of radial-spectroscopic imaging to provide fast noninvasive access to the distribution of various chemical constituents for histochemistry of plants with cylindrical stem symmetry. A given cylindrical symmetry of an object can be exploited in spectroscopic imaging to shorten the experiment time dramatically. A radial-chemical-shift image of sugar in *A. heyneanus* has been presented. It reveals the correct radial distribution of the metabolite and correct spectra. The time savings allows application of radial-correlation-peak imaging without unacceptably long experiment times. The short experiment time for radial-chemical-shift imaging will also allow acquisition of dynamic studies on metabolites in plants with cylindrical stem symmetry. The application of radial-correlation-peak imaging to the plant *A. heyneanus* led to the discovery of an yet unidentified metabolite. This proves the value of radial-spectroscopic imaging for the investigation of the metabolism of plants.

ACKNOWLEDGMENTS

This study was financially supported by grants received from the Deutsche Forschungsgemeinschaft (Graduiertenkolleg NMR Ha 1232/8-4, M.v.K. Ki 433/2-2).

REFERENCES

1. A. A. Maudsley, A. Oppelt, and A. Ganssen, *Siemens Forsch. Entwicklungsber.* **8**(6) (1979).
2. T. R. Brown, B. M. Kincaid, and K. Ugurbil, *Proc. Natl. Acad. Sci. U.S.A.* **79,** 3523 (1982).
3. P. R. Luyten, A. J. H. Marien, W. Heindel, P. H. J. van Gerwen, K. Herholz, J. A. den Hollander, G. Friedmann, and W. D. Heiss, *Radiology* **176,** 791 (1990).
4. C. M. Segebarth, D. F. Baleriaux, P. R. Luyten, and J. A. den Hollander, *Magn. Reson. Med.* **13,** 62 (1990).
5. C. T. W. Moonen, G. Sobering, P. C. M. van Zijl, J. Gillen, M. von Kienlin, and A. Bizzi, *J. Magn. Reson.* **92,** 556 (1992).
6. R. S. Menon, K. Hendrich, X. Hu, and K. Ugurbil, *Magn. Reson. Med.* **26,** 368 (1992).
7. H. Kolem, R. Sauter, M. G. Friedrich, M. Schneider, K. Wicklow, and K. Bachman, Abstracts of the Society of Magnetic Resonance in Medicine, 12th Annual Meeting, p. 1096, 1993.
8. H. P. Hetherington, D. J. E. Luney, J. T. Vaughan, J. W. Pan, S. L. Ponder, O. Tschendel, D. B. Twieg, and G. M. Pohost, *Magn. Reson. Med.* **33,** 427 (1995).
9. H. Rumpel and J. M. Pope, *Magn. Reson. Imaging* **10,** 187 (1992).
10. A. Metzler, W. Köckenberger, M. von Kienlin, E. Komer, and A. Haase, *J. Magn. Reson. B* **105,** 249 (1994).
11. A. Metzler, M. Izquierdo, A. Ziegler, W. Köckenberger, E. Komer, M. von Kienlin, A. Haase, and M. Décorps, *Proc. Natl. Acad. Sci. U.S.A.* **92,** 1 (1995).
12. A. Ziegler, A. Metzler, W. Köckenberger, M. Izquierdo, E. Komer,

A. Haase, M. Décorps, and M. von Kienlin, *J. Magn. Reson. B* **112,** 141 (1996).

13. A. Ziegler, M. von Kienlin, Y. le Fur, C. Rubin, M. Décorps, and C. Rémy, ''Congrès du Group de Recherche sur les Applications due Magnetisme en Médecine 1996.''
14. S. Y. Lee and Z. H. Cho, *Magn. Reson. Med.* **12,** 56 (1989).
15. D. H. Lee and S. Lee, *Magn. Reson. Imaging* **12,** 613 (1994).
16. P. D. Majors and A. Caprihan, *J. Magn. Reson.* **94,** 225 (1991).
17. M. Meininger, P. M. Jakob, M. von Kienlin, and A. Haase, Abstracts of the Society of Magnetic Resonance, Third Scientific Meeting, p. 1900, 1995.
18. G. Bringmann and F. Pokorny, *in* ''The Alkaloids,'' Vol. 46, p. 127, Academic Press, New York, 1995.
19. Y. S. Schiffenbauer, C. Tempel, R. Abramovitch, G. Meier, and M. Neeman, *Cancer Res.* **55,** 153 (1995).
20. R. N. Bracewell, ''The Fourier Transform and Its Applications,'' 2nd ed. revised, p. 244, McGraw–Hill, New York, 1986.
21. A. Haase, J. Frahm, W. Hänicke, and D. Matthaei, *Phys. Med. Biol.* **30,** 341 (1985).
22. Y. Le Fur, A. Ziegler, D. Bourgeois, M. Decorps, and C. Remy, *Magn. Reson. Med.* **29,** 431 (1993).
23. M. von Kienlin, C. T. W. Moonen, A. van der Toorn, and P. C. M. van Zijl, *J. Magn. Reson.* **93,** 423 (1991).